



SENSORCOMM 2024

The Eighteenth International Conference on Sensor Technologies and Applications

ISBN: 978-1-68558-207-4

November 3rd - 7th, 2024

Nice, France

SENSORCOMM 2024 Editors

Jaime Lloret, Universitat Politècnica de València, Spain

SENSORCOMM 2024

Forward

The Eighteenth International Conference on Sensor Technologies and Applications (SENSORCOMM 2024), held on November 3-7, 2024, was a multi-track event covering related topics on theory and practice on wired and wireless sensors and sensor networks.

Sensors and sensor networks have become a highly active research area because of their potential of providing diverse services to broad range of applications, not only on science and engineering, but equally importantly on issues related to critical infrastructure protection and security, health care, the environment, energy, food safety, and the potential impact on the quality of all areas of life.

Sensor networks and sensor-based systems support many applications today on the ground. Underwater operations and applications are quite limited by comparison. Most applications refer to remotely controlled submersibles and wide-area data collection systems at a coarse granularity.

In wireless sensor and micro-sensor networks energy consumption is a key factor for the sensor lifetime and accuracy of information. Protocols and mechanisms have been proposed for energy optimization considering various communication factors and types of applications. Conserving energy and optimizing energy consumption are challenges in wireless sensor networks, requiring energy-adaptive protocols, self-organization, and balanced forwarding mechanisms.

We take here the opportunity to warmly thank all the members of the SENSORCOMM 2024 technical program committee, as well as all the reviewers. The creation of such a high quality conference program would not have been possible without their involvement. We also kindly thank all the authors who dedicated much of their time and effort to contribute to SENSORCOMM 2024. We truly believe that, thanks to all these efforts, the final conference program consisted of top quality contributions.

We also thank the members of the SENSORCOMM 2024 organizing committee for their help in handling the logistics and for their work that made this professional meeting a success.

We hope that SENSORCOMM 2024 was a successful international forum for the exchange of ideas and results between academia and industry and to promote further progress in the area of sensor technologies and applications. We also hope that Nice provided a pleasant environment during the conference and everyone saved some time to enjoy the historic charm of the city.

SENSORCOMM 2024 Chairs

SENSORCOMM 2024 Steering Committee

Anne-Lena Kampen, Western Norway University of Applied Sciences, Norge
Masanari Nakamura, Hokkaido University, Japan

SENSORCOMM 2024 Publicity Chair

Lorena Parra Boronat, Universitat Politecnica de Valencia, Spain
Laura Garcia, Universidad Politécnica de Cartagena, Spain

SENSORCOMM 2024

Committee

SENSORCOMM 2024 Steering Committee

Anne-Lena Kampen, Western Norway University of Applied Sciences, Norge
Masanari Nakamura, Hokkaido University, Japan

SENSORCOMM 2023 Publicity Chair

Lorena Parra Boronat, Universitat Politècnica de Valencia, Spain
Laura Garcia, Universidad Politécnica de Cartagena, Spain

SENSORCOMM 2024 Technical Program Committee

Majid Bayani Abbasy, National University of Costa Rica, Costa Rica
Younes Adriouch, Mohammed Five University of Rabat (UM5R), Agdal, Rabat, Morocco
Yassine Al-Amrani, Abdelmalek Essaadi University, Tetuan, Morocco
Amin Al-Habaibeh, Nottingham Trent University, UK
Jesús B. Alonso Hernández, Institute for Technological Development and Innovation in Communications (IDeTIC) | University of Las Palmas de Gran Canaria (ULPGC), Spain
Youssef N. Altherwy, Imperial College London, UK
Mário Alves, Politécnico do Porto - School of Engineering (ISEP), Portugal
Thierry Antoine-Santoni, University of Corsica, France
Kazutami Arimoto, Okayama Prefectural University, Japan
Anish Arora, The Ohio State University / The Samraksh Company, USA
Andy Augousti, Kingston University London, UK
Karim Baïna, Université Mohammed V de Rabat, Morocco
Michel Bakni, ESTIA Recherche, Bidart, France
Hind Bangui, Masaryk University, Czech Republic
Michail J. Beliatis, Aarhus University, Denmark
Boutaina Benhmimou, Mohammed Five University of Rabat (UM5R), Agdal, Rabat, Morocco
Reda Benkhouya, Ibn Tofail University, Morocco
Abdelmadjid Bouabdallah, University of Technology of Compiègne, France
Souheila Bouam, University of Batna 2, Algeria
An Braeken, Vrije Universiteit België, Belgium
Seddik Bri, Higher School of Technology - Moulay Ismail University, Meknes, Morocco
Alessandro Brighente, University of Padova, Italy
Juan-Vicente Capella-Hernández, Universitat Politècnica de València, Spain
Oscar Carrasco Quilis, Casa Systems Inc., Valencia, Spain
Vítor Carvalho, 2Ai Lab- School of Technology - IPCA / Algoritmi Research Center - Minho University, Portugal
Mario Cifrek, University of Zagreb, Croatia
Luis J. de la Cruz Llopis, Universitat Politècnica de Catalunya, Spain
Baban P. Dhonge, Indira Gandhi Center for Atomic Research, Kalpakkam, India
Alexis Duque, Rtone, Lyon, France
Nabil El Akkad, ENSA | Sidi Mohamed Ben Abdellah University, Morocco

Loubna El Amrani, Ibn University Tofail Kénitra, Morocco
Mohamed El Bakkali, Mohammed V University of Rabat (UM5R), Agdal, Rabat, Morocco
Karim El Moutaouakil, Sidi Mohamed Ben Abdellah University Fez | Polydisciplinary Faculty of Taza, Morocco
Youssef Elgholb, University Sidi Mohamed Ben Abdellah, Fez, Morocco / Technical University of Cartagena, Spain
Yasyn Elyusufi, Abdelmalek Essaadi University, Morocco
Fatima Zahra Fagroud, Hassan II University of Casablanca, Morocco
Biyi Fang, Microsoft Corporation, USA
Stefan Fischer, University of Lübeck, Germany
Fernando Juan García-Diego, Universitat Politècnica de València, Spain
Dinesh R. Gawade, Tyndall National Institute | University College Cork, Ireland
Alireza Ghasempour, University of Applied Science and Technology, Iran
Lyamine Guezouli, University of Batna 2, Algeria
Arda Gumusalan, IBM, USA
Mostafa Hanoune, Hassan 2 University of Casablanca, Morocco
Agostino Iadicicco, University of Naples Parthenope, Italy
Miao Jin, University of Louisiana at Lafayette, USA
Anand Y. Joshi, Parul University, India
Grigoris Kaltsas, University of West Attica, Greece
Anne-Lena Kampen, Western Norway University of Applied Sciences, Norge
Lutful Karim, Seneca College of Applied Arts and Technology, Toronto, Canada
Azeddine Khiat, ENSET Mohammedia | University Hassan II of Casablanca, Morocco
André Kokkeler, University of Twente, Netherlands
Boris Kovalerchuk, Central Washington University, USA
Sathish Kumar, Hanyang University, South Korea
Hanane Lamaazi, Khalifa University of Science and Technology, Abu Dhabi, United Arab Emirates
Wenjuan Li, The Hong Kong Polytechnic University, Hong Kong
Yi Li, Security Lancaster | Lancaster University, UK
Chiu-Kuo Liang, Chung Hua University, Hsinchu, Taiwan
David Lizcano, Madrid Open University (UDIMA), Spain
Giuseppe Loseto, LUM "Giuseppe Degennaro" University, Italy
Flaminia Luccio, University Ca' Foscari of Venice, Italy
Tahir Mahmood, International Islamic University Islamabad, Pakistan
Abdalah Makhoul, University of Franche-Comté, France
Stefano Mariani, Politecnico di Milano, Italy
Jose-Manuel Martinez-Caro, Technical University of Cartagena, Spain
Lucas M. C. e Martins, Brazilian Institute of Teaching, Development, and Research (IDP) / University of Brasília / Estácio of Brasília, Brazil
Carlo Massaroni, Università Campus Bio-Medico di Roma, Italy
Michele Mastroianni, University of Salerno, Italy
Lei Mei, KLA Corporation, USA
Weizhi Meng, Technical University of Denmark, Denmark
Carosena Meola, University of Naples Federico II, Italy
Ahmad Mohamad Mezher, University of New Brunswick, Canada
Fabien Mieyeville, Polytech Lyon - University Claude Bernard Lyon 1, France
Raúl Monroy, Tecnológico de Monterrey, Mexico
Rafael Morales Herrera, Universidad de Castilla-La Mancha, Spain

Masanari Nakamura, Hokkaido University, Japan
Dmitry Namiot, Lomonosov Moscow State University, Russia
Jagriti Narang, Jamia Hamdard, New Delhi, India
Mir Mohammad Navidi, West Virginia University, USA
Seyedeh Masoumeh Navidi, Wayne State University, Detroit, USA
Michael Niedermayer, Berliner Hochschule für Technik, Germany
Rosdiadee Nordin, UniversitiKebangsaan Malaysia, Malaysia
Bogdan Oancea, University of Bucharest, Romania
Brendan O'Flynn, Tyndall National Institute | University College Cork, Ireland
Fouad Omari, Mohammed Five University of Rabat (UM5R), Agdal, Rabat, Morocco
Pouya Ostovari, San Jose State University | Charles W. Davidson College of Engineering, USA
Carlos Enrique Palau Salvador, Universitat Politècnica de València, Spain
Lorenzo Palazzetti, University of Perugia, Italy
Bruno Pereira dos Santos, University of Ouro Preto, Brazil
Ivan Miguel Pires, Instituto de Telecomunicações - Universidade da Beira Interior / Polytechnic Institute of Viseu, Portugal
Patrick Pons, LAAS-CNRS, France
Giuseppe Prencipe, University of Pisa, Italy
Càndid Reig, University of Valencia, Spain
Girish Revadigar, Huawei International Pte Ltd, Singapore
Christos Riziotis, National Hellenic Research Foundation, Greece
Lorenzo Rubio Arjona, Universitat Politècnica de València, Spain
Ulrich Rückert, Bielefeld University, Germany
Sain Saginbekov, Nazarbayev University, Nut-Sultan, Kazakhstan
Prasan Kumar Sahoo, Chang Gung University, Taiwan
Addisson Salazar, Universitat Politècnica de València, Spain
Hooman Samani, University of Hertfordshire, UK
Sevil Sen, Hacettepe University, Turkey
Nadir Shah, COMSATS University Islamabad, Wah Campus, Pakistan
F. M. Javed Mehedi Shamrat, University of Malaya, Kuala Lumpur, Malaysia
Sheng Shen, University of Illinois at Urbana-Champaign, USA
Sahbi Sidhom, Lorraine University & LORIA Lab., France
Francesco Betti Sorbelli, University of Perugia, Italy
Mu-Chun Su, National Central University, Taiwan
Alvaro Suárez Sarmiento, University of Las Palmas de Gran Canaria, Spain
Hicham Gibet Tani, Abdelmalek Essaadi University, Tetouan, Morocco
Shrikant Tangade, University of Padova, Italy / CHRIST University, India
Rui Teng, Qilu Normal University, China
Daniel Tokody, Óbuda University | NextTechnologies Ltd. Complex Systems Research Institute, Hungary
Hicham Toumi, Higher School of Technology-Sidi Bennour | Chouaïb Doukkali University, El Jadida, Morocco
Carlos Travieso González, University of Las Palmas de Gran Canaria, Spain
Yu Chee Tseng, NCTU, Taiwan
Eirini Eleni Tsiropoulou, University of New Mexico, USA
Stefan Valentin, Darmstadt University of Applied Sciences, Germany
Manuela Vieira, CTS/ISEL/IPL, Portugal
Shuai Wang, Southeast University, China
Wenwu Wang, University of Surrey, UK

You-Chiun Wang, National Sun Yat-sen University, Taiwan
Murat Kaya Yapici, Sabanci University, Turkey
Hong Yang, Nokia Bell Labs, Murray Hill, USA
Sergey Y. Yurish, International Frequency Sensor Association (IFSA), Spain
Zhenghao Zhang, Florida State University, USA
Ying Zhao, University of Melbourne, Australia
Zhe Zhou, Huzhou University, China
Chengzhi Zong, eBay Inc, USA

Copyright Information

For your reference, this is the text governing the copyright release for material published by IARIA.

The copyright release is a transfer of publication rights, which allows IARIA and its partners to drive the dissemination of the published material. This allows IARIA to give articles increased visibility via distribution, inclusion in libraries, and arrangements for submission to indexes.

I, the undersigned, declare that the article is original, and that I represent the authors of this article in the copyright release matters. If this work has been done as work-for-hire, I have obtained all necessary clearances to execute a copyright release. I hereby irrevocably transfer exclusive copyright for this material to IARIA. I give IARIA permission to reproduce the work in any media format such as, but not limited to, print, digital, or electronic. I give IARIA permission to distribute the materials without restriction to any institutions or individuals. I give IARIA permission to submit the work for inclusion in article repositories as IARIA sees fit.

I, the undersigned, declare that to the best of my knowledge, the article does not contain libelous or otherwise unlawful contents or invading the right of privacy or infringing on a proprietary right.

Following the copyright release, any circulated version of the article must bear the copyright notice and any header and footer information that IARIA applies to the published article.

IARIA grants royalty-free permission to the authors to disseminate the work, under the above provisions, for any academic, commercial, or industrial use. IARIA grants royalty-free permission to any individuals or institutions to make the article available electronically, online, or in print.

IARIA acknowledges that rights to any algorithm, process, procedure, apparatus, or articles of manufacture remain with the authors and their employers.

I, the undersigned, understand that IARIA will not be liable, in contract, tort (including, without limitation, negligence), pre-contract or other representations (other than fraudulent misrepresentations) or otherwise in connection with the publication of my work.

Exception to the above is made for work-for-hire performed while employed by the government. In that case, copyright to the material remains with the said government. The rightful owners (authors and government entity) grant unlimited and unrestricted permission to IARIA, IARIA's contractors, and IARIA's partners to further distribute the work.

Table of Contents

Fluid Flow Speed Measurement System Using Fiber Bragg Grating Temperature Sensor Based on Microwave Heating <i>Atsushi Yurai</i>	1
Easy-to-use Wireless Sensor Network Simulator for Estimating Power Consumption and Communication Availability <i>Yuta Hosokawa, Minoru Tanaka, and Kazuki Nakamura</i>	4
NNEPS: Network-Updated E-Paper Signage with Reduced Standby Power Consumption <i>Takafumi Akiba and Tsubasa Yumura</i>	8
Shoe Recognition Model with Floor Pressure Sensors <i>Sora Kamimura, Tetsuo Yutani, Atsuko Shibuya, and Tsubasa Yumura</i>	10

Fluid Flow Speed Measurement System Using Fiber Bragg Grating Temperature Sensor Based on Microwave Heating

Atsushi Yarai

Department of Electrical, Electronic and Information Engineering
Faculty of Engineering, Osaka Sangyo University
3-1-1 Nakagaito, Daito, Osaka 574-8530 Japan
e-mail: yarai@osaka-sandai.ac.jp

Abstract—A fluid flow speed measurement system using a Fiber Bragg Grating (FBG) temperature sensor based on microwave heating is proposed. The technique of this system features contamination-free operation with fluids, due to its adoption of platinum electrodes for non-contact microwave heating and the use of FBG fiber made of fused quartz. The results demonstrate that sensing linearity could be achieved. This capability is in nearly perfect accord with the sensing characteristics of conventional flow sensors using a thermal method.

Keywords- flow speed measurement; FBG sensor; fiber ring laser; microwave heating; thermal flow meter.

I. INTRODUCTION

Recently, the necessity of new techniques for measuring low fluid flow speeds has been recognized [1]. For example, to maintain acceptable quality control, it is necessary to precisely control extremely low speeds of injecting solutions [1]. Furthermore, each approach to extremely low-speed measurement using conventional techniques, such as Doppler methods and ultrasonics, has its particular difficulties. This is because such means cannot achieve detection of changes in physical parameters due to the extremely low speed. Consequently, thermal techniques have previously been applied for this purpose, and several sensor device configurations have been proposed, developed, and commercialized [2]. This technique is adequate for extremely low-speed measurement, but there remain several unresolved fundamental problems, such as chemical contamination, mixing of debris at the sensing element, and durability. In medical applications, such problems pose the risk of fatal consequences.

This paper proposes the construction of a fluid flow speed measurement system using a Fiber Bragg Grating (hereinafter referred to as FBG) temperature sensor based on microwave heating. Basically, such systems have extremely complex configurations, and they are very expensive for use in a sensor system. On the other hand, the proposed sensor has distinctive features including contamination-free operation with fluids, due to its adoption of platinum electrodes for non-contact microwave heating and the use of FBG fiber made of fused quartz; moreover, a flow-cell can certainly be made of quartz. Additionally, the mixing of debris at the sensing element into the fluid can be almost entirely eliminated. As the first step, in this article, a sensing principle is described and a system configuration is proposed. Next, experimental data obtained

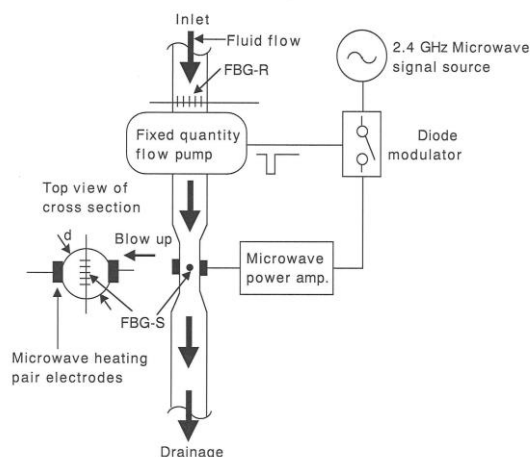
from closed cycle water flow are shown. Finally, the measuring capabilities are briefly discussed.

II. MEASUREMENT SYSTEM CONFIGURATION

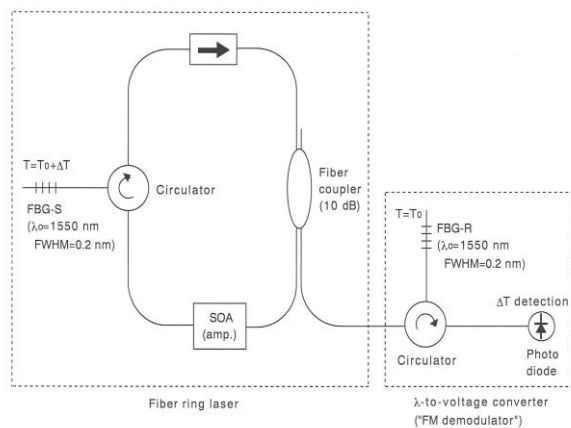
Figures 1 (a) and (b) show the experimental apparatus in a laboratory, prior to designing the prototype sensor, and its fiber optical system composed of a fiber ring laser, respectively. The details of the fluid flow system are described in the next section, while this section mainly addresses the optical system. In the configuration of this apparatus, the following two FBG sensors are assembled to function independently as temperature measurement elements. FBG-R (reference) operates as a steady fluid temperature sensing element, converting the change in wavelength to that in the amplitude of the laser beam, as shown on the right side of Figure 1 (b). FBG-S (sense) functions as a sensing element of the transition temperature change induced by the microwave heating, and this is applied to a wavelength tunable device using a fiber ring laser, as shown on the left side of Figure 1 (b) [3].

The microwave heating electrodes are situated across from each other, enclosed in the fluid flow tube with a diameter of 2 mm, and FBG-S is mounted in the center of the tube's interior. Here, FBG functions adequately for high electromagnetic fields because the optical device is manufactured solely of fused quartz. The microwave with a frequency of 2.45 GHz is fed between the two electrodes after the signal power is boosted to approximately 2 W by a power amplifier. The frequency of 2.45 GHz was chosen due to regulations in Japan's radio law. Here, the combination of FBG-R and FBG-S, each with a reflection wavelength of 1550 nm, has certain advantages, as follows. Even with a steady fluid temperature, the offset temperature changes; however, this change and the wavelength transition induced by it normally cancel each other due to the differential effect achieved by combining these FBGs.

The fiber ring laser shown in Figure 1 (b) contains the Semiconductor Optical Amplifier (SOA; Thorlabs SOA1013S) for compensating the optical loss inside the ring loop, resulting in laser oscillation. The linewidth of this laser is found by adopting a self-delayed heterodyne interferometry method. As a result, a linewidth of a few MHz was obtained. This spectrum is absolutely a straight line without any uncertainty, when considering the spectrum of FBG-R to have a full width at half maximum of 0.2 nm. The laser beam branched by a fiber coupler is reflected by the FBG-R and then fed to a photo diode. The block composed of the circulator, FBG-R, and photo diode is equivalent to a demodulator used for "optical wavelength modulation."



(a) Fluid flow system and configuration of sensing elements.



(b) Fiber ring laser of sensing demodulator.

Figure 1. Experimental apparatus in laboratory (prototype sensor).

III. MEASUREMENT RESULTS AND DISCUSSION

The prepared fixed-quantity flow pump shown in Figure 1 (a) alternates in its operation mode like a “heartbeat” between the charge (suction mode) and discharge (extrusion mode) of fluid in the cylinder. The volume of the cylinder was fixed to 7.5 ml constantly in this pump, using the ability to control the flow speed by adjusting the time of discharge. The microwave heating is toggled to active in extrusion mode and to dormant in suction mode, and a PIN diode modulator is installed for these operations. Figure 2 shows an example of a signal’s waveform detected by the photo diode. The signal of the upper wave is driven by the PIN modulator, operating in the above two modes. When the fluid flowed to the flow cell is cut off in suction mode, the FBG-S detects the transition change in temperature, corresponding to the lower wave form drawn. The peak-to-peak vale of the lower wave form indicates the magnitude of temperature change.

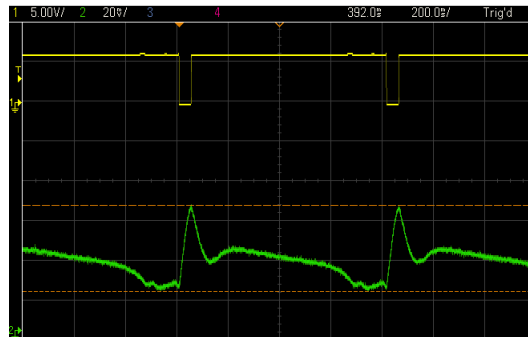


Figure 2. Typical waveform of detected signal (lower).

Figure 3 shows an example of the water flow rate dependence of the detected signal’s amplitude. As can be seen in the figure, it was demonstrated that the sensing linearity could be obtained when the flow rate was between approximately 0.2 and 1.5 ml per second. This result corresponds almost perfectly with the sensing characteristics of a conventional flow sensor using a thermal method, i.e., the temperature of the flow medium is negatively proportional to its flow rate. On the other hand, the amplitude of the detected signal decreased dramatically when the flow rate was below 0.2 ml per second. The reason for this is assumed to be as follows. At first, the temperature of the fluid rises sharply due to an exceedingly low flow speed. Next, the recovery time of returning to the temperature prior to heating becomes longer due to the thermal capacity of the fluid after microwave heating is halted. Thus, the alternating of temperatures is suppressed, which certainly decreases the detected signal’s amplitude to a low level. It is important to optimally adjust the power of the microwave.

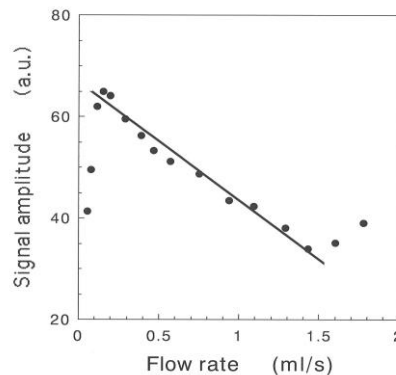


Figure 3. Water flow rate dependence of detected signal’s amplitude.

IV. CONCLUSION AND FUTURE WORK

A new fluid flow speed measurement system using a fiber Bragg grating temperature sensor based on microwave heating was proposed. The key feature of this system is the combination of microwave heating and an FBG temperature sensor having a high electromagnetic field. Consequently, the system is free of chemical contamination due to the use of only platinum and fused quartz. Furthermore, results demonstrate that sensing linearity could be achieved. This capability is in nearly perfect

accord with the sensing characteristics of conventional flow sensors using a thermal method. As future work, we will address the system design and optimization of several parameters, such as microwave power and the mounting positions of FBGs, to expand the dynamic range of measurement. After that, we will compare the sensing characteristics of the proposed method in accord with the conventional flow sensors.

REFERENCES

- [1] P. Fiala, R. Kadlec, and J. Zúkal, "Measuring Fluid Flow Velocities in the Context of Industry 4.0" 12th International Conference on Measurement, Aug. 2019, pp. 295-298, doi: 10.23919/MEASUREMENT47340.2019.8780025.
- [2] F. Ejeian et al., "Design and applications of MEMS flow sensors: A review" *Sensor Actuator A Phys*, vol. 295, pp. 483-502, Aug. 2019.
- [3] W. Xie, Y. Zhang, P. Wang, and J. Wang, "Optical Fiber Sensors Based on Fiber Ring Laser Demodulation Technology" *Sensors (Basel)*, vol. 18(2), Feb. 2018, pp. 505-530, doi: 10.3390/s18020505.

Easy-to-use Wireless Sensor Network Simulator for Estimating Power Consumption and Communication Availability

Yuta Hosokawa, Minoru Tanaka, Kazuki Nakamura

Information and Communication Technology Division

Railway Technical Research Institute

Kokubunji, Tokyo, 185-8540 Japan

e-mail: {hosokawa.yuta.84, tanaka.minoru.96, nakamura.kazuki.26}@rtri.or.jp

Abstract—In order to enable comparison and determination of node placement and modulation methods when introducing wireless sensor networks in railway environments, we developed an easy-to-use simulator. The simulator models the fixed-cycle transmission of sensor data and estimates communication paths and battery consumption on the network. The simulator is designed to be easily accessed from a web browser and parameters can be easily configured. This paper introduces the simulation model and implementation, as well as several examples of simulation results.

Keywords—*wireless sensor network; simulator; routing; power consumption.*

I. INTRODUCTION

In recent years, there are high demands from Japanese railway operators to introduce more efficient and labor-saving technologies for the maintenance of railway equipment. One solution is to apply Wireless Sensor Networks (WSNs) to monitor the condition of equipment scattered along railways remotely. By using WSNs to collect equipment condition monitoring data, it is possible to reduce the need for frequent on-site inspections. When applying this principle, the following elements must be considered: communication range, modulation method, power consumption, and implementation of battery power supply. Each element affects the others, and multiple options are available, making it challenging for railway operators to design optimal WSNs.

Several network simulators are widely used to design optimal WSNs. Network Simulator-2 (ns-2) [1], Network Simulator-3 (ns-3) [2], and OMNeT++ [3] offer powerful tools for network simulation. These simulators can include power consumption modeling through additional modules. For instance, Energy Framework [4] for ns-3 and INET Framework for OMNeT++ provides extensions for simulating power consumption. However, these simulators typically require advanced technical expertise for command-line operations or custom scripting, making them challenging for non-technical stakeholders like railway operators.

This paper presents a user-friendly simulator designed to estimate the communication quality and battery consumption of WSNs in railway environments. Our tool supports multi-hop transmissions and mesh networking for nodes extending over long distances along railways. Featuring a web-based Graphical User Interface (GUI), the simulator allows users to easily set parameters, compare node placements and

communication methods, and view results instantly. Our simulator meets the specific needs of WSN deployment planning in railway maintenance operations without requiring specialized software or technical expertise.

The rest of this paper is as follows. Section II describes the design of the simulation model. Section III shows the implementation of the simulator and simulation results. Section IV argues about the benefits and future work of the simulator. Finally, Section V concludes the article.

II. DESIGN OF SIMULATION MODEL

A. Node Types and Placement

In this model, a “node” consists of a radio transceiver, a microcontroller, a battery, and sensors. An arbitrary number of nodes can be placed on the simulation field.

Each node is classified into the following three roles, based on the Wi-SUN Field Area Network (FAN) model [1] to support multi-hop transmissions.

- **Border Router (BR):**
A node that acts as a boundary with the external network and manages the entire network. Sensor data acquired by each node is aggregated to the BR, which transmits the data to a central unit or other devices via the external network. In the simulation, exactly one BR is required to be placed.
- **Router node:**
A node with sensing and relay functionality, capable of relaying packets from distant router and leaf nodes that cannot directly communicate with the BR.
- **Leaf node:**
A terminal node whose main objective is to measure and collect sensor data for transmission. The leaf node does not have relay functionality.

In the developed simulator, the position of a node is represented in a fixed X-Y coordinate [m]. Antenna height [m] and gain [dBi] are also specified for each node. The transmission power [dBm] is set to a common value for all nodes. Also, the node can be set to either with an external power supply or battery-powered, in which case battery capacity [mAh] is also specified.

Leaf and router nodes periodically transmit sensor data to the BR. In the simulation, the size of this data [bytes] and the transmission cycle [sec] may be specified for each node. When applying the WSN to real-world scenarios, the contents

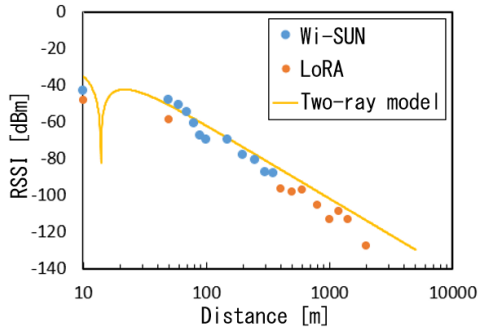


Figure 1. Relationship between the distance and RSSI

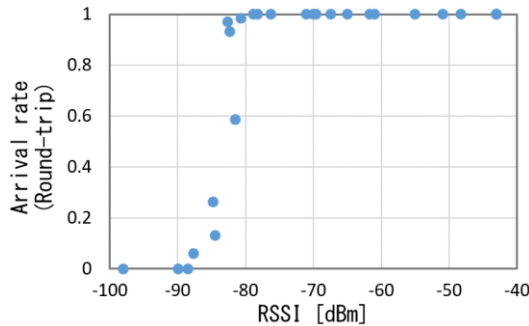


Figure 2. Relationship between RSSI and the arrival rate

of each sensor and data size may differ, so the data size and transmission cycle can be set to different values for each node.

B. Estimation of Communication Coverage

To build an estimation model of the communication coverage, we conducted an experiment to obtain basic data on radio communications. On a straight viaduct, we measured the Received Signal Strength Indicator (RSSI) and data arrival rate while varying the distance between two nodes. The relationship between the distance and RSSI for Wi-SUN and LoRa in the 920 MHz band is shown in Figure 1. We confirmed that the obtained RSSI generally matches the results estimated by the two-ray ground-reflection model [6] regardless of the modulation method. The relationship between RSSI and the data arrival rate for Wi-SUN is shown in Figure 2. While RSSI is above a certain value, the data arrival rate is close to 100%. In contrast, when RSSI is below that value, the arrival rate decreases significantly.

From these results, our simulator applies the two-ray ground-reflection model to estimate the RSSI value for each pair of nodes. Whenever an estimated RSSI value exceeds the pre-defined threshold, communication is deemed possible. The threshold value should be determined by actual measurements or expectations about environmental factors such as noise level.

C. Simulation of Routing

All router and leaf nodes have to determine a transmission path towards the BR to collect and/or distribute data. The simulator determines the transmission path from each node to the BR using the Routing Protocol for Low-Power and Lossy Networks (RPL). RPL is a routing protocol for selecting an appropriate route among multiple possible routes. It is used in

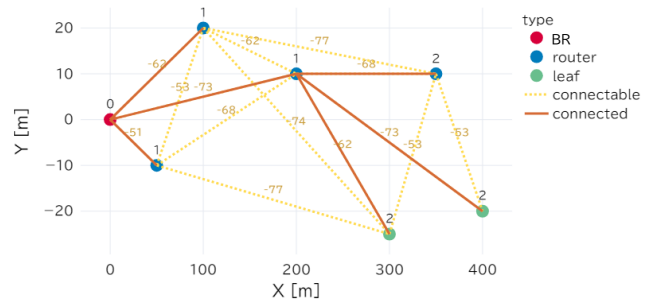


Figure 3. Example of routing

Wi-SUN and other networks capable of multi-hop transmission. In RPL, a Destination-Oriented Directed Acyclic Graph (DODAG) is constructed based on an objective function that defines the criteria for route selection. For example, the objective function of Wi-SUN FAN is calculated using the hop count and time series data of arrival rate [1]. Since our simulation model assumes a static communication environment, we use a simple algorithm that considers the hop counts and RSSI. The details are described below:

- 1) Assign Rank = 0 to the BR, where Rank is the number of edges that pass through to reach the BR.
- 2) Assign Rank = 1 to the nodes that can communicate directly with the BR (Rank = 0) and adopt a route that directly connects these nodes to the BR.
- 3) Assign Rank = 2 to the nodes that can communicate with a node with Rank = 1 but whose route has not yet been determined. If there are multiple candidates, the route with the highest RSSI value is adopted.
- 4) In the same way, the nodes that can communicate with the node with Rank = k but the route is not yet determined are set to Rank = k+1.

Figure 3 shows an example of routing simulation. Seven nodes are placed on a simulation field and the yellow dashed lines represent edges where communication is estimated to be possible. The numbers show the estimated RSSI and the orange lines represent the selected route. The number above each node is the Rank value. For example, there are two nodes with Rank = 1 that the upper right router node (Rank = 2) can connect to, but the node in the middle with the higher RSSI value (-68 > -77) is selected as the parent. The leaf node in the lower right can be connected to two router nodes, but the node with the smaller Rank value is selected as the parent to minimize the number of hops.

D. Estimation of Power Consumption

The simulator estimates battery consumption for each battery-powered node. The estimation is based on a model with a constant voltage output. To calculate the total battery consumption over time, we sum up the current [mA] drawn at each moment. This gives us the cumulative charge used, measured in [mAh].

The model of the current consumption is shown in Figure 4. Each node is assumed to consume c_{wait} [mA] during the time it is not transmitting data, and c_{tx} [mA] during data transmission. Since the current consumption may differ depending on the node type, these parameters can be changed for each node type. For example, a leaf node saves power by

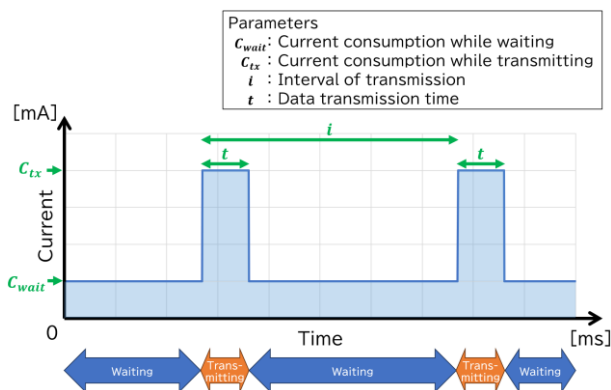


Figure 4. Current Consumption model

putting the transceiver to sleep when it is not transmitting, while a router node should always be on standby for reception.

To calculate the cumulative power consumption, it is necessary to determine the transmission time t [msec] per data. Generally, the transmission time increases linearly with the data size. Therefore, in our simulation model, it is expressed as $t = ax + b$, where x [bytes] is the data size to be transmitted. The parameters a and b are common values in the simulation based on actual measurements with wireless modules. This model assumes that each node transmits data once every i [sec], which is set for each node. In multi-hop transmissions, the router node is required to transmit both its own sensor data and the data received from its child nodes to the parent node, resulting in higher power consumption.

III. IMPLEMENTATION OF THE SIMULATOR

A. Implementation of the Simulator

Based on the model described in Section II, we developed a simulator for WSNs that considers both data transmission and power consumption. The simulator was implemented in Python 3.11 using the Streamlit 0 library to enable GUI controls. Streamlit is an open-source Python library for creating web-based GUIs. The simulator was developed on a Linux server and made accessible through a specific URL, allowing users to interact with it via a web browser on any PC connected to the private network. The simulator consists of three components described below:

1) Parameter input interface

The simulator provides a web-based interface for users to input all necessary parameters. These include:

- Node placement and characteristics (Section II. A)
- Communication availability estimation (Section II. B)
- Power consumption estimation (Section II. D)

The interface features real-time updates, where changes in input values are instantly reflected in the corresponding graphs, facilitating rapid iteration of simulation parameters.

2) Network and Communication Path Visualization

The simulator generates a visual representation based on input parameters, illustrating:

- Node placement
- Inter-node communication availability
- Data transmission routes to BR

A dynamic timeline feature allows users to simulate battery consumption over time. This includes dynamic re-routing when nodes deplete their batteries.

3) Time-series analysis of battery capacity

The simulator provides a graph depicting the relationship between the elapsed time and the remaining battery capacity for each node. Key features include:

- Simulation continues until all battery capacity is depleted.
- Time resolution set to 1 day, optimized for planning battery replacement strategies for WSN deployments.
- Visualization of long-term network behavior without battery replacement.

B. Example of Running Simulation

1) Example simulation for Wi-SUN

We simulated a WSN including multi-hop transmissions under the assumption of Wi-SUN. Node placement is as shown in Figure 3. The BR is connected to an external power source and the other nodes are connected to 10000-mAh batteries. Each router and leaf node has an antenna height of 1.5 m and is set to transmit 16 bytes of data at 5-sec intervals. The transmission power of each node is 13 dBm. The parameters of data transmission time and current consumption values were based on the pre-measurement using ROHM's Wi-SUN evaluation module BP35C5-T01.

The simulation results are shown in Figure 5. At the beginning of the simulation (Day 0, as in Figure 3), nodes 4 to 6 used node 3 as the relay node, leading to rapid battery depletion in node 3 (Day 65). Afterward, they switched to node 2, which also ran out of battery by Day 78.

From these results, it can be said that nodes that relay information from distant nodes consume a particularly large amount of power and are likely to run out of battery power. Furthermore, under the same conditions, we conducted a simulation assuming that only node 3 could connect to an external power source, resulting in which all nodes could connect to the BR until Day 79.

2) Example simulation for LoRa

We conducted a trial simulation assuming a Long Range Wide Area Network (LoRaWAN) [8]. It is possible to simulate a network that is limited to a star topology like LoRaWAN by considering a gateway as BR and other end nodes as leaf nodes. One BR and six leaf nodes are placed and each leaf node has an antenna height of 1.5 m and a battery capacity of 10000 mAh. The transmission data size is set to a common value of 16 bytes for each node, and data transmission intervals are set to 5 sec for nodes 1 to 3 and 10 sec for nodes 4 to 6. The transmission power is 13 dBm. The parameters of transmission time and current consumption values were based on the datasheet of a LoRa wireless module.

The simulation results are shown in Figure 6. Initially (Day 0), all the leaf nodes are connected to the BR. Nodes 1 to 3, with shorter transmission intervals, ran out of battery earlier (Day 108), followed by all nodes running out of battery on Day 215. The LoRa module sleeps the transceiver during standby, resulting in very low power consumption. On the other hand, due to the long time it takes to transmit data, nodes that transmit data frequently run out of battery quickly.

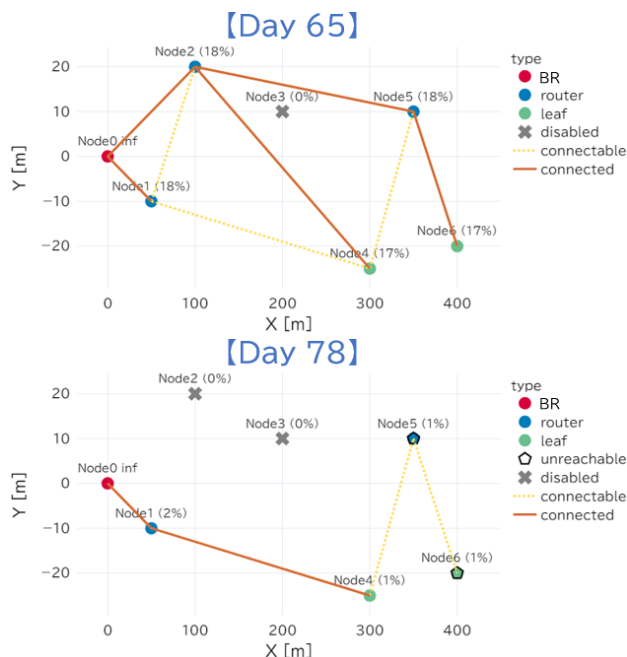


Figure 5. Results of example simulation for Wi-SUN

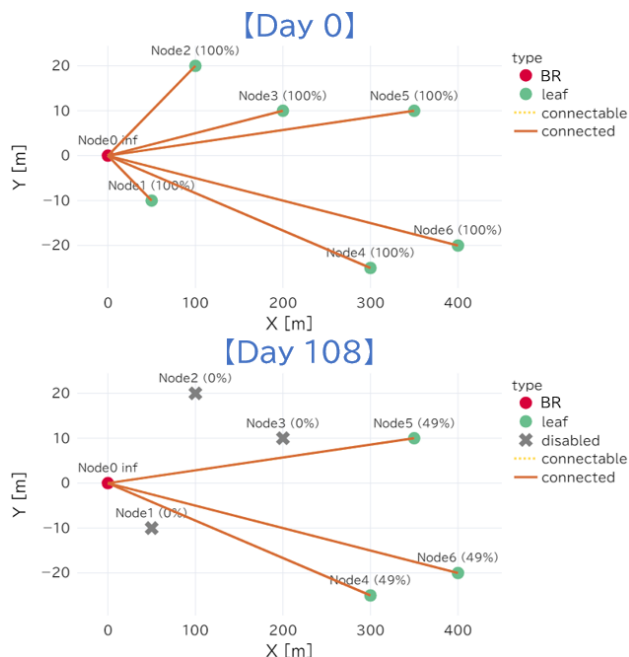


Figure 6. Results of example simulation for LoRa

IV. DISCUSSION

The simulator we developed allows for easy estimation of data transmission paths and battery operating days in WSNs by simply inputting the sensor locations and battery capacities. In comparison to existing simulators such as ns-2, ns-3, and OMNeT++, our tool offers advantages in ease of use and real-time visualization. Users can configure parameters and view simulation results instantly without extensive technical knowledge through a web browser-based interface. This feature particularly benefits railway operators who need to design and evaluate networks quickly and effectively.

Our simulator’s real-time feedback on power consumption and communication path visualization enables quick identification of nodes requiring external power or are at risk of battery depletion. This interactive functionality distinguishes our approach from the more static, script-based methods of traditional simulators.

However, there are several areas where we can enhance the accuracy and functionality. Future improvements aim to address:

- Incorporating terrain and railway equipment
- Simulating retransmission operation based on arrival rate estimation
- Supporting more advanced routing algorithms
- Modeling modules with multiple state transitions, such as sleep, receive standby, and data transmission

V. CONCLUSION

To enable comparison and determination of node placement and modulation methods for the introduction of WSNs in railway environments, we developed an easy-to-use simulator. This simulator estimates communication paths and

battery consumption on the network. It models the fixed-cycle transmission of sensor data using the locations of wireless sensors, antenna performance, and battery capacity as input parameters. The simulator can simulate not only star networks but also mesh networks, such as Wi-SUN. Designed for ease of access, the simulator can be operated from a web browser, and parameters can be easily configured.

In the future, we plan to build a WSN using actual wireless modules to verify the accuracy and effectiveness of the simulator’s estimates. Additionally, we aim to improve the model to accommodate more modulation methods and enhance estimation accuracy.

REFERENCES

- [1] The Network Simulator - ns-2, <https://www.isi.edu/websites/nsnam/ns/> [retrieved: October, 2024]
- [2] ns-3 | a discrete-event network simulator for internet systems, <https://www.nsnam.org/> [retrieved: October, 2024]
- [3] V. András and R. Hornig, “An overview of the OMNeT++ simulation environment,” 1st International ICST Conference on Simulation Tools and Techniques for Communications, Networks and Systems, 2010.
- [4] H. Wu, S. Nabar, and R. Poovendran, “An Energy Framework for the Network Simulator 3 (ns-3),” 4th International ICST Conference on Simulation Tools and Techniques, 2012.
- [5] R. Hirakawa, K. Mizutani, and H. Harada, “Specification and Performance Analysis of Wi-SUN FAN,” IEEE Open Journal of Vehicular Technology, vol. 4, pp. 849-866, 2023.
- [6] Edited and supervised by Y. Hosoya, “Radiowave Propagation Handbook (in Japanese),” Realize Inc. Tokyo, pp. 125–126, 1999.
- [7] Streamlit | A faster way to build and share data apps, <https://streamlit.io/> [retrieved: October, 2024]
- [8] About LoRaWAN | LoRa Alliance, <https://loralliance.org/about-lorawan/> [retrieved: October, 2024]

NNEPS: Network-Updated E-Paper Signage with Reduced Standby Power Consumption

Takafumi Akiba and Tsubasa Yumura

Hokkaido Information University

Ebetsu, Japan

e-mail: s2481102@do-johodai.ac.jp, yumu@yumulab.org

Abstract—Electronic Paper Signage (EPS) is used in various ways, such as at bus stops and in menu lists. One type of EPS is a network-updated EPS that updates content via the Internet. In the network update type EPS, a management computer consumes power constantly while awaiting contents. Therefore, a feature of the electronic paper (e-paper), namely, that it does not require standby power, cannot be utilized. To solve this problem, we proposed a network-updated EPS system that reduces power consumption during standby communication. We developed a prototype of the proposed EPS system and evaluated its power consumption.

Keywords—Electronic Paper, Signage, Power Saving.

I. INTRODUCTION

Electronic Paper Signage (EPS) is a type of digital signage. EPS is a signage specialized in displaying still images using an electronic paper display. Electronic paper displays are characterized by low power consumption because they can retain the screen without consuming power after updating the screen. EPS is being used for floor guides [1] and information boards in office buildings [2].

One type of EPS is a network-updated EPS that updates content via the Internet [3]. Network-updated EPSs are used at bus stops and at certain types of bulletin boards [3]. In the network-updated EPS, the computer that controls the e-paper consumes power constantly while waiting for contents. Therefore, an important characteristic of the e-paper, namely, that it does not require standby power, cannot be utilized. To solve this problem, we propose a network-updated EPS that reduces power consumption during standby. The rest of the paper is structured as follows. In Section II, we present the related work. In Section III, we describe the proposed method. Section IV describes the system configuration and Section V the implementation. In Section VI we conduct the assessment of the power reduction. Finally, we conclude in Section VII.

II. RELATED WORK

Tobias *et al.* [4] have developed a prototype and investigated the performance of an information display device that combines photovoltaics, a low-power wireless protocol, and an electronic paper display. Their results showed that low-resolution e-paper displays can achieve numerous screen updates with very limited energy.

Yang *et al.* [5] proposed two different power supply methods for e-paper: in-situ triboelectric and wireless power supply within 30 cm. They showed that each method can successfully

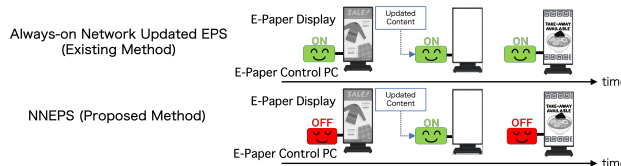


Figure 1. Comparison of the existing and proposed methods.

update the screen and drive the e-paper without using batteries or power supply modules.

III. PROPOSED METHOD

In this study, a network-updated EPS is converted to a normally-off to save power. Normally-off [6] is the concept of turning off the power when a system is not in use.

The network-updated EPS waits for updated content sent via the Internet. The control PC built into the EPS is responsible for the process of receiving and displaying content on the e-paper display. In existing network-updated EPSs, the control PC is always running and consuming power. Conversely, in the proposed method, the control PC is turned off. When updating content, the control PC is activated upon receiving a notification. When the update of the e-paper display is completed, the control PC is turned off. In this way, the control PC spends less time in the startup state, thereby reducing power consumption. We named the system that realizes EPS with normally-off network electronic paper signage Normally-off Network Electronic Paper Signage (NNEPS). Figure 1 shows a comparison of the NNEPS with the existing network-updated EPS.

IV. SYSTEM CONFIGURATION

The NNEPS is composed of an e-paper, an e-paper control PC, and a power control plug. The electronic paper is the display part. The e-paper control PC performs processing related to e-paper updates. The power control plug stands by with the communication function turned on and turns the power supply to the e-paper control PC on and off as needed for screen updates, thereby enabling the EPS to achieve normally-off.

V. IMPLEMENTATION

Figure 2 shows the NNEPS. The NNEPS implements a power control plug using a microcontroller and relay module.



Figure 2. A picture of the NNEPS.

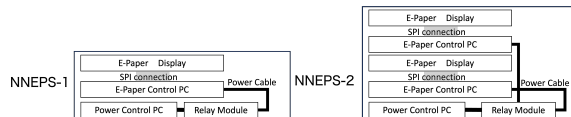


Figure 4. Configuration diagram of NNEPS-1 and NNEPS-2.

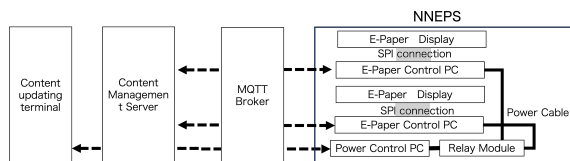


Figure 3. Configuration chart of the NNEPS System

The M5Stack Core2 for AWS (Amazon Web Services) was used as the micro-controller that controlled the relay modules. The M5Stack implements firmware that turns the relay module on and off in response to notifications via MQTT (Message Queuing Telemetry Transport).

Figure 3 shows the system configuration of the NNEPS. Multiple EPSs can be connected using relay modules to manage power on/off status.

VI. ASSESSMENT OF POWER REDUCTION

In order to compare the power consumption resulting from different screen update control flows, experiments will be conducted using the same hardware, and no comparison will be made with existing solutions. We conducted an experiment to evaluate the power consumption of the NNEPS and that of the existing network-updated EPS. Each system was prepared, and the power consumption of each system was measured using a watt checker. The power consumption of NNEPS is the sum of the power consumed by the e-paper control PC and the power supply control PC. The NNEPS measured power for two different cases, one with one EPS connected to the relay module and the other with two EPSs connected to the relay module. The NNEPS with one EPS connected to the relay module is designated as NNEPS-1, and the NNEPS with two EPSs connected to the relay module is designated as NNEPS-2 (Figure 4). The frequency of screen refreshes was set to once every five minutes, and power consumption was measured for one hour.

Figure 5 shows the results of the evaluation experiment. The power consumption was 1.88 Wh for the existing method in which the e-paper control PC was always active, and 1.25 Wh for NNEPS-1. Under these conditions, the proposed method, NNEPS-1, reduced the amount of electricity by about 33% compared to the existing method. The value for NNEPS-2 was 2.81 Wh, which is more than twice the value for NNEPS-1. This result is considered an implementation convenience.

When multiple EPSs are controlled by the NNEPS, screen updates are performed one by one, so the time required for the

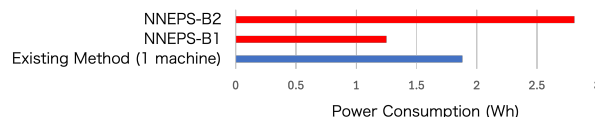


Figure 5. Power consumption comparison between existing and proposed methods.

screen update process increases with the number of connected units. NNEPS-1 completes the screen update process in an average of 85 seconds, but when two EPSs are connected, the process takes an average of 108 seconds. In the case of NNEPS-2, both e-paper control PCs are turned off when the screen update process of the EPS to be updated later is completed. Therefore, the power consumption of both of the two e-paper control PCs increased due to the longer startup time, and is considered to be more than twice as much as when one of the PCs is connected.

VII. CONCLUSION

NNEPS reduces the number of PCs that are always on standby for communication, it is more effective the more EPSs there are. In this implementation, a maximum of two EPSs could be connected, but screen update processing could not be performed in parallel, resulting in unnecessary power consumption. In the future, we will work on implementation to increase the number of EPSs controlled by NNEPS and aim to compare with existing products.

ACKNOWLEDGMENTS

This research was supported by the Hokkaido IT Creator Discovery and Development Project (Shinsetsu Program) conducted by Shinsetsu, a general incorporated association. We would like to express our sincere appreciation.

REFERENCES

- [1] CREA Co., *Office building guide - crea co., ltd. | world's largest 42-inch electronic paper signage*, <https://www.crea2007.co.jp/pr/20230211c/>, retrieved: Sep. 2024, (online).
- [2] TintTech, *Wired & wireless epaper digital signage - tinttech*, <https://tinttech.io/>, [retrieved: Sep., 2024], (online).
- [3] Alpha Japan, *E paper signage*, <https://www.a-japan.co.jp/epd/eps.html>, [retrieved: Sep., 2024], (online).
- [4] T. Grosse-Puppendahl *et al.*, "Exploring the design space for energy-harvesting situated displays," *UIST '16*, pp. 41–48, 2016. DOI: 10.1145/2984511.2984513.
- [5] Y. Bo-Ru *et al.*, "Battery-free charging methods for driving e-paper devices," in *Proceedings of the International Display Workshops*, 2020, p. 751.
- [6] T. Nakada, T. Shimizu, and H. Nakamura, "Normally-off computing for IoT systems," in *2015 International SoC Design Conference (ISOC)*, 2015, pp. 147–148. DOI: 10.1109/ISOC.2015.7401761.

Shoe Recognition Model with Floor Pressure Sensors

Sora Kamimura

Hokkaido Information University
Ebetsu, Japan

e-mail: s2321083@do-johodai.ac.jp

Tetsuo Yutani

Atsuko Shibuya
FirstFourNotes, LLC
Tokyo, Japan

e-mail: tyutani@firstfournotes.com
ashibuya@firstfournotes.com

Tsubasa Yumura

Hokkaido Information University
Ebetsu, Japan

e-mail: yumu@yumulab.org

Abstract—In research on traffic flow analysis, computer vision methods using camera images have been the predominant approach. However, using cameras for flow line analysis presents challenges, such as creating blind spots caused by obstructions such as people or objects. Additionally, privacy concerns arise. These issues can be mitigated using floor pressure sensors for flow line analysis. To successfully perform flow line analysis with these sensors, it is essential to identify individuals based on factors such as weight, stride length, speed, and shoe type. In this study, we developed a system to identify shoe types from footprint pressure distribution using a neural network model. Our focus was on three types of shoes: sneakers, room shoes, and sandals. We collected data for each category and created a recognition model, achieving an F-measure of 97.6% in the best model. The primary challenges for practical implementation are measurement time and durability.

Keywords—Sensors, Neural networks, Flow Line Analysis, Pressure-Sensitive Conductive Sheet.

I. INTRODUCTION

Traffic flow analysis in environments such as retail stores, factories, warehouses, and public facilities is crucial for enhancing productivity and mitigating risks. In response to these needs, several image recognition methods using cameras have been proposed in recent years [1]. Although these camera-based methods offer the benefit of using existing surveillance infrastructure, they have considerable drawbacks, including difficulties in detecting overlapping people or objects, which can create blind spots. Additionally, the installation of cameras is often hindered by privacy concerns. However, these challenges can be circumvented using floor pressure sensors as an alternative to cameras, which effectively address both blind spots and privacy issues.

The pressure-sensitive conductive sheet Velostat can be used to create pressure sensors for installation on floors [2]. Velostat has the characteristic of reducing resistance when pressure is applied, allowing for pressure measurements based on changes in voltage. The benefits of Velostat include its low cost, ease of arrangement modifications, high density of measurement points, and excellent portability.

In a previous study on object identification using pressure sensors with Velostat, Yuan *et al.* [3] successfully identified ten different objects, including Lego pieces, a bottle, and an iron block. However, there have been no studies using Velostat-based pressure sensors for flow line analysis.

To perform traffic flow analysis, it is essential to determine whether footprints originate from the same individual. Identifying a person through their footprints involves analyzing

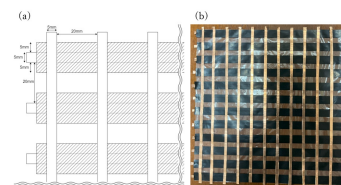


Figure 1. (a) Structure of pressure sensor (b) Created pressure sensor.

various factors, including weight, stride length, walking speed, and shoe type. In this study, we developed a floor pressure sensor using Velostat and a neural network model using sensor data to identify footwear.

The rest of the paper is structured as follows. In Section II, we present the pressure sensor. In Section III, we describe the recognition model. Section IV has the results and discussion. We conclude the article in Section V.

II. PRESSURE SENSOR

The pressure sensors used in this research were constructed using Velostat, copper foil tape, and an Arduino platform.

The sensor we developed has copper foil tapes that are 5 mm wide and spaced 20 mm apart, arranged in a grid formation consisting of 12 tapes both vertically and horizontally, totaling 144 measurement points (Figure 1).

For power transmission, the Arduino's digital pin is directly connected to the copper foil tape aligned parallel to the strip of Velostat. For data reception, the copper foil tape located at the point where it intersects vertically with the strip of Velostat is connected directly to the Arduino's analog pin to measure voltage, which is then linked to ground through a 1 k Ω resistor.

Pressure is measured using the following procedure. First, the Arduino sequentially sends electrical signals to the 12 copper foil tapes positioned parallel to the Velostat. Next, Arduino measures the voltage across all the copper foil tapes on the opposite side while supplying electricity to each individual tape. This process is repeated every 100 ms.

III. RECOGNITION MODEL

A. Structure of the neural network model

The neural network model used for identification is structured with an input layer, three hidden layers, and an output layer. The input layer takes in raw sensor data, comprising $12 \times 12 = 144$ nodes. Each of the three hidden layers is a fully connected layer, containing $6 \times 6 = 36$ nodes. The output layer



Figure 2. Shoes used for data collection.

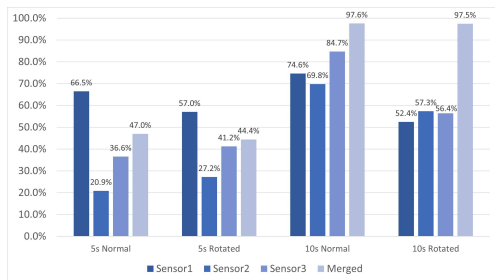


Figure 3. F-measure graph.

generates probabilities for each of the three types of shoes: sneakers, room shoes, and sandals. The model uses Rectified Linear Unit (ReLU) as the activation function for all layers. The optimizer employed is Stochastic Gradient Descent, set with a learning rate of 0.8, whereas the loss function used is cross-entropy loss.

B. Collection of Training Data

Three types of shoes were selected for classification: sneakers, room shoes, and sandals (Figure 2). A 1.5 kg weight was placed inside each shoe.

During the data collection process, the sensor was first calibrated for at least 5 s without any weight. The shoe was then placed on the sensor and allowed to rest for a few seconds before measuring the pressure distribution.

Each shoe underwent this measurement process 50 times, resulting in a total of 150 data points per sensor. Additionally, there were two different waiting times (5 and 10 s) between placing the shoe on the sensor and measuring the pressure. In total, 900 data points were collected, comprising two waiting times and three sensors. We refer to this collection as the normal dataset. We also created a rotated dataset by rotating the normal dataset 90, 180, and 270 degrees. Furthermore, we created a merged dataset that consolidated the data without differentiating between sensors.

The collected data were split into training, validation, and test sets with a random distribution. The ratio for all datasets is 70:15:15.

IV. RESULTS AND DISCUSSION

Figure 3 shows the F-measure for each dataset.

During a waiting period of 10 s, both normal and rotated measurements exceed 5 s. Possible reasons for this include unresolved noise, such as vibrations generated when the shoe is placed on the sensor, which may not dissipate in 5 s, and insufficient power from the Arduino, which can delay voltage recovery.

For each sensor, measurements under normal conditions during the 10-s waiting period were higher than rotated data. This occurs because the sensor’s sensitivity characteristics become more pronounced over time. While the model can estimate sensitivity bias using normal data, it struggles with data from rotated measurements. Factors contributing to this biased sensitivity may include non-uniform resistance of the Velostat, errors in sensor fabrication, and degradation from use.

This sensor has been designed primarily for traffic flow analysis. In practical traffic flow analysis, multiple sensors will be deployed, making it impractical to retrain the model with each new sensor. Therefore, using the rotated data method for data collection is advantageous because it mitigates the risk of sensor sensitivity bias and facilitates an easy increase in the training dataset.

V. CONCLUSION

In this paper, we developed a pressure sensor using a pressure-sensitive conductive sheet called Velostat coupled with a neural network model to identify different types of shoes. We performed experiments with three different shoe types. The trained model achieved an impressive F-measure of 97.6%. Using a rotated dataset proved to be the most effective approach for real-world applications because it involved rotating the data every 90 degrees, thereby eliminating sensitivity bias from each sensor.

The following challenges may arise when performing an actual flow line analysis. In this study, experiments were performed using 1.5 kg weights placed inside the shoe. However, the pressure readings could surpass the measurable range when an individual walks on the sensor. To obtain accurate pressure distribution, measurements were recorded several seconds after placing the shoe on the sensor. However, this waiting period is not practical in real-world analyses. Additionally, while this research used three different types of shoes, there are many more types in reality, some of which are more difficult to identify.

To address the issues identified in this research and improve our responses to projected situations, we will further develop the following sensors and applications: a sensor with improved response time and durability, a system capable of managing multiple sensor errors, and a system that can identify individuals based on various feature values.

REFERENCES

- [1] L. Hou, W. Wan, K. Han, R. Muhammad, and M. Yang, “Human detection and tracking over camera networks: A review,” in *2016 International Conference on Audio, Language and Image Processing*, IEEE, 2016, pp. 574–580.
- [2] S. Suprpto, A. Setiawan, H. Zakaria, W. Adiprawita, and B. Supartono, “Low-cost pressure sensor matrix using velostat,” *2017 5th International Conference on Instrumentation, Communications, Information Technology, and Biomedical Engineering*, pp. 137–140, 2017.
- [3] L. Yuan, H. Qu, and J. Li, “Velostat sensor array for object recognition,” *IEEE Sensors Journal*, vol. 22, no. 2, pp. 1692–1704, 2021.